# Porous $CeO_X$/SiC Nanocomposites Prepared from Reverse Polycarbosilane-Based Microemulsions

Emanuel Kockrick,[†] Piotr Krawiec,[†] Uwe Petasch,[‡] Hans-Peter Martin,[‡] Mathias Herrmann,[‡] and Stefan Kaskel*,[†]

*Department of Inorganic Chemistry, Technical University of Dresden, Mommsenstrasse 6, D-01062 Dresden, Germany, and Fraunhofer-Institute for Ceramic Technologies and Systems IKTS, Winterbergstrasse 28, D-01277 Dresden, Germany*

*Received June 20, 2007. Revised Manuscript Received October 16, 2007*

Reverse microemulsions consisting of aqueous cerium nitrate solution as the internal phase and polycarbosilane dissolved in heptane as the continuous phase were used as a precursor for the controlled synthesis of dispersed cerium oxide particles inside a porous SiC matrix. According to dynamic light scattering experiments, the effective diameter of the cerium hydroxide particles obtained after ammonia addition is effectively controlled in a range of 2–10 nm with the molar water/surfactant ratio ($R_w$ = 6–16). Pyrolysis at 1200 to 1500 °C produces materials with specific surface areas up to 240 $m^2\ g^{-1}$. Whereas crystallization of the matrix is achieved only at higher temperature, cerium oxide particles form agglomerates composed of smaller nanoparticles that tend to dissolve into the ceramic matrix at 1500 °C leaving macropores behind. The high specific surface area is attributed to the presence of mesopores with a broad size distribution. Excess carbon present after pyrolysis is removed by oxidation at 900 °C causing a significant decrease of the surface area for high surface area materials, whereas intermediate surface area materials (50–100 $m^2\ g^{-1}$) show a high textural stability.

## Introduction

Inverse microemulsions are used for the preparation of nanoparticles and nanostructures.[1] They allow to precisely define the particle diameter by changing the micelle size. The latter can be easily achieved by adjusting the chemical composition of the reactant mixture (e.g., $R_W$, molar ratio of water to surfactant; Scheme 1).[2,3] Successful preparation of various metal,[4,5] oxide,[6–9] sulfide,[10,11] or other chalcogenide nanoparticles[12,13] via the microemulsion technique is reported in the literature. Typically alkoxides,[2,14] chlorides, and nitrates[15] are used as precursors. The nanoparticles can be further used in powder form or be redispersed in another medium.[16] Especially, the addition of inorganic nanoparticles into polymers is of high interest.[2,14,17] Such an incorporation into the polymer can also be achieved by in situ *generation* using the monomer as the oil phase. After particle formation, the monomers can be polymerized to form the polymer matrix with well dispersed inorganic nanoparticles introducing new functions into the polymer material.[17]

In the following, we describe the direct preparation of cerium oxide nanoparticles inside silicon carbide polymer precursors via the microemulsion technique. Recently, we have shown that in situ techniques can also be used for the preparation of noble metal nanoparticles (Pt, Pd) inside a mesoporous silica matrix using normal micelles.[18] Cerium oxide is an important oxidation catalyst and is used commercially for burning the carbon combustion residues (soot) from diesel engine exhaust.[19,20] In combination with transition metals, it can be used as a water−gas shift catalyst.[21,22] In several reports, the microemulsion technique was applied

* Corresponding author. Phone: 49-351-46333632. Fax: 49-351-46337287. E-mail: stefan.kaskel@chemie.tu-dresden.de.
[†] Technical University of Dresden.
[‡] Fraunhofer-Institute for Ceramic Technologies and Systems IKTS.

(1) Uskokovic, V.; Drofenik, M. *Surf. Rev. Lett.* **2005**, *12*, 239.
(2) Althues, H.; Kaskel, S. *Langmuir* **2002**, *18*, 7428.
(3) Henle, J.; Simon, P.; Frenzel, A.; Scholz, S.; Kaskel, S. *Chem. Mater.* **2007**, *19*, 366.
(4) Yadav, O. P.; Palmqvist, A.; Cruise, N.; Holmberg, K. *Colloids Surf., A* **2003**, *221*, 131.
(5) Chen, F. X.; Xu, G. Q.; Hor, T. S. A. *Mater. Lett.* **2003**, *57*, 3282.
(6) Masui, T.; Fujiwara, K.; Machida, K.; Adachi, G.; Sakata, T.; Mori, H. *Chem. Mater.* **1997**, *9*, 2197.
(7) Stathatos, E.; Lianos, P.; DelMonte, F.; Levy, D.; Tsiourvas, D. *Langmuir* **1997**, *13*, 4295.
(8) Herrig, H.; Hempelmann, R. *Nanostruct. Mater.* **1997**, *9*, 241.
(9) Beck, C.; Hartl, W.; Hempelmann, R. *J. Mater. Res.* **1998**, *13*, 3174.
(10) Natarajan, U.; Handique, K.; Mehra, A.; Bellare, J. R.; Khilar, K. C. *Langmuir* **1996**, *12*, 2670.
(11) Agostiano, A.; Catalano, M.; Curri, M. L.; Della Monica, M.; Manna, L.; Vasanelli, L. *Micron* **2000**, *31*, 253.
(12) Foos, E. E.; Stroud, R. M.; Berry, A. D. *Nano Lett.* **2001**, *1*, 693.
(13) Quinlan, F. T.; Kuther, J.; Tremel, W.; Knoll, W.; Risbud, S.; Stroeve, P. *Langmuir* **2000**, *16*, 4049.
(14) Palkovits, R.; Althues, H.; Rumplecker, A.; Tesche, B.; Dreier, A.; Holle, U.; Fink, G.; Cheng, C. H.; Shantz, D. F.; Kaskel, S. *Langmuir* **2005**, *21*, 6048.
(15) Bumajdad, A.; Zaki, M. I.; Eastoe, J.; Pasupulety, L. *Langmuir* **2004**, *20*, 11223.
(16) Althues, H.; Simon, P.; Kaskel, S. *J. Mater. Chem.* **2007**, *17*, 758.
(17) Althues, H.; Palkovits, R.; Rumplecker, A.; Simon, P.; Sigle, W.; Bredol, M.; Kynast, U.; Kaskel, S. *Chem. Mater.* **2006**, *18*, 1068.
(18) Krawiec, P.; Kockrick, E.; Auffermann, G.; Simon, P.; Kaskel, S. *Chem. Mater.* **2006**, *18*, 2663.
(19) Miro, E. E.; Ravelli, F.; Ulla, M. A.; Cornaglia, L. M.; Querini, C. A. *Catal. Today* **1999**, *53*, 631.
(20) Trovarelli, A. *Catal. Rev.- Sci. Eng.* **1996**, *38*, 439.
(21) Fu, Q.; Weber, A.; Flytzani-Stephanopoulos, M. *Catal. Lett.* **2001**, *77*, 87.
(22) Fu, Q.; Saltsburg, H.; Flytzani-Stephanopoulos, M. *Science* **2003**, *301*, 935.

10.1021/cm071657n CCC: $40.75 
Published on Web 12/05/2007

**Scheme 1. Schematic Synthesis Procedure for $CeO_X$−SiC Composites in Five Steps**[a]

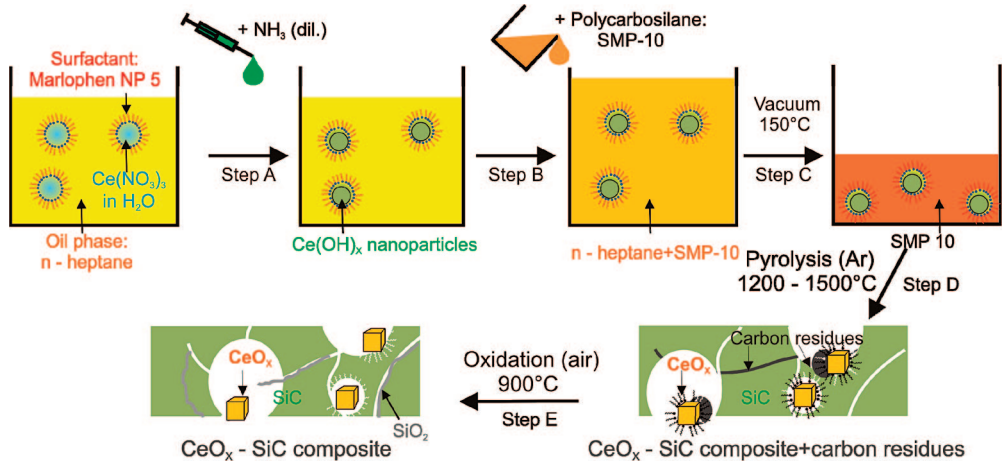


[a] Starting system consisting of inverse microemulsion with aqueous cerium precursor, (A) precipitation of nanoscale $Ce(OH)_3$ particles inside micelle structure by adding diluted ammonia, (B) addition of liquid polycarbosilane SMP-10 in oil phase, (C) removal of volatile compounds and cross-linking of polycarbosilane, (D) pyrolysis in argon inert atmosphere at 1200−1500 °C to form SiC, and (E) oxidative treatment to remove residual carbon.

for the preparation of nanoscale ceria systems.[15,23–26] However, for high temperature catalytic applications such as soot combustion, the stabilization of the active catalyst nanoparticles (e.g., ceria) inside an inert matrix is necessary to minimize sintering and agglomeration. Therefore, porous silicon carbide ceramics are attractive catalyst supports because they possess excellent thermal conductivity, hardness, and high mechanical stability.[27–29] In particular, silicon carbide is a promising material for the stabilization of nanoparticles at high temperatures. SiC is already used in commercial soot filter systems.[20,24,30] High surface area mesoporous silicon carbide (up to 800 $m^2\ g^{-1}$) can be prepared via chemical vapor deposition or nanocasting of ordered mesoporous silica.[31–35] However, the stability of high surface area SiC in oxidative conditions at high temperatures is relatively low because of the surface passivation by silica formation.[36] Thus, for applications at high temperatures and in oxidative environments, moderate specific surface areas (50–100 $m^2\ g^{-1}$) are preferred.

The principle of the direct synthesis of cerium oxide in the silicon carbide matrix using inverse microemulsions is shown in Scheme 1. An aqueous cerium nitrate solution is solubilized in the reverse micelle core (nonionic Marlophene NP5 surfactant is used, Scheme 1) while heptane is the continuous oil phase. In the first step, cerium hydroxide is precipitated by the addition of ammonia (Scheme 1, step A), and afterward liquid polycarbosilane (SiC precursor) is added (Scheme 1, step B). Solvents like heptane and water are removed subsequently in vacuum (Scheme 1, step C); thus, a polycarbosilane/cerium hydroxide nanoparticle/Marlophen NP5 mixture is obtained. This mixture is then used as a precursor for the direct preparation of $CeO_X$/SiC nanocomposites (Scheme 1, step D). The nanocomposites were oxidized to remove the carbon residues resulting from the incomplete surfactant removal and decomposition into elemental carbon (Scheme 1, step E).

The resulting $CeO_X$/SiC nanocomposites have moderate surface areas (up to 240 $m^2\ g^{-1}$). The specific surface area is controlled with the chemical composition and the pyrolysis temperature. The nature of cerium oxide is dependent on the pyrolysis temperature and can be in nanocrystalline form or as an amorphous phase.

## Experimental Section

**Synthesis of Polycarbosilane/Cerium Hydroxide Composite.** All chemicals were used as received. A 6.7 g portion of an aqueous 0.2 M $Ce(NO_3)_3$ solution ($Ce(NO_3)_3 \cdot 6H_2O$, Aldrich, 99%), 68 g of *n*-heptane (Sigma-Aldrich, >99%), and a defined mass of the nonionic surfactant Marlophen NP 5 ($RO(CH_2CH_2O)_xH$, $x = 5$, R = nonylphenyl, $M = 440\ g \cdot mol^{-1}$, SASOL) were mixed according to $R_W$ values at 25 °C as listed in Table 1.

The viscosity of all transparent microemulsions was measured after 1 h at 25 °C with Ubbelohde viscosimeters type 532-13Ic by Schott. The mean value of five measurements is given. The microemulsion systems containing cerium salt were stirred for 1 h in a closed 250 mL flask at 25 °C. Then, 0.25 g (A samples)/0.5 g (B samples) of diluted ammonia solution (Sigma-Aldrich, 2.5 wt %) were added dropwise to the transparent microemulsion system and stirred for an additional 1 h at 25 °C. The liquid polycarbosilane precursor SMP-10 (Starfire Systems) was added to the ternary phase system in defined mass ratios of 37:1 and 18.5:1 (according to the theoretical SiC to $CeO_2$ ratio and in the following identified as A and B). To remove the volatile compounds water and *n*-heptane,

(23) Zhang, J.; Ju, X.; Wu, Z. Y.; Liu, T.; Hu, T. D.; Xie, Y. N.; Zhang, Z. L. *Chem. Mater.* **2001**, *13*, 4192.
(24) Masui, T.; Fujiwara, K.; Peng, Y. M.; Sakata, T.; Machida, K.; Mori, H.; Adachi, G. *J. Alloy. Compd.* **1998**, *269*, 116.
(25) Martinez-Arias, A.; Fernandez-Garcia, M.; Ballesteros, V.; Salamanca, L. N.; Conesa, J. C.; Otero, C.; Soria, J. *Langmuir* **1999**, *15*, 4796.
(26) Fernandez-Garcia, M.; Martinez-Arias, A.; Iglesias-Juez, A.; Belver, C.; Hungria, A. B.; Conesa, J. C.; Soria, J. *J. Catal.* **2000**, *194*, 385.
(27) Mitomo, M.; Kim, Y. W.; Hirotsuru, H. *J. Mater. Res.* **1996**, *11*, 1601.
(28) Sternitzke, M. *J. Eur. Ceram. Soc.* **1997**, *17*, 1061.
(29) Ledoux, M. J.; Pham-Huu, C. *CATTECH* **2001**, *5*, 226.
(30) Yao, H. C.; Yao, Y. F. Y. *J. Catal.* **1984**, *86*, 254.
(31) Krawiec, P.; Weidenthaler, C.; Kaskel, S. *Chem. Mater.* **2004**, *16*, 2869.
(32) Krawiec, P.; Geiger, D.; Kaskel, S. *Chem. Commun.* **2006**, 2469.
(33) Lu, A. H.; Schmidt, W.; Kiefer, W.; Schüth, F. *J. Mater. Sci.* **2005**, *40*, 5091.
(34) Pol, V. G.; Pol, S. V.; Gedanken, A. *Chem. Mater.* **2005**, *17*, 1797.
(35) Shi, Y. F.; Meng, Y.; Chen, D. H.; Cheng, S. J.; Chen, P.; Yang, T. F.; Wan, Y.; Zhao, D. Y. *Adv. Funct. Mater.* **2006**, *16*, 561.
(36) Krawiec, P.; Kaskel, S. *J. Solid State Chem.* **2006**, *179*, 2281.

**Table 1. Sample Codes, Composition, and Viscosities of the Microemulsion Systems Used**

| sample name | $R_W$ | $M(SiC)/m(CeO_2)$ | $m_{n\text{-heptane}}$ [g] | $m_{Ce(NO_3)_3,aq}$ [g] | $m_{Marlophen}$ [g] | viscosity [cP] | $m_{NH_3,dil}$ [g] | $m_{SMP\text{-}10}$ [g] |
|---|---|---|---|---|---|---|---|---|
| A5.8 | 5.8 | 37:1 | | | 24.6 | 2.96 | | 8.9 |
| A7.7 | 7.7 | | | | 18.6 | 2.13 | | |
| A11.7 | 11.7 | 37:1 | 68.0 | 6.7 | 12.3 | 1.06 | 0.25 | 8.9 |
| A13.8 | 13.8 | | | | 10.4 | 0.87 | | |
| A16.4 | 16.4 | 37:1 | | | 8.9 | 0.76 | | 8.9 |
| B16.4 | 16.4 | 18.5:1 | 136 | 13.5 | 17.8 | 0.76 | 0.5 | 9.0 |

**Table 2. Temperature Program for Pyrolyzing the Polycarbosilane/Cerium Hydroxide Composite under an Argon Atmosphere**

| | temperature ramp | | | | | | |
|---|---|---|---|---|---|---|---|
| | 1 | 2 | 3 | 4 | 5 | 6 | 7 |
| target temperature [°C] | 80 | 400 | 600 | 900 | 1200/1350/1500 | 750 | 50 |
| heating ramp [°C·h$^{-1}$] | 200 | 60 | 60 | 120 | 240 | 300 | 250 |
| time [h] | 0 | 1 | 0.5 | 1 | 2 | 0.1 | |

the clear solutions were concentrated using a rotary evaporator at temperatures up to 150 °C at 80 mbar.

**Thermal Treatment: Pyrolysis and Oxidative Passivation.** Pyrolysis of the polycarbosilane/cerium hydroxide composite was conducted in Ar 5.0 flow (3 L min$^{-1}$) in a horizontal tubular alumina furnace (Gero HTRH 70-300) with the seven temperature ramps listed in Table 2.

To remove residual carbon, the pyrolyzed $CeO_X$−SiC composite was post-treated at 900 °C for 30 min with a heating ramp of 10 °C·min$^{-1}$ in a muffle furnace under a static air atmosphere.

**Characterization.** The inverse microemulsion systems were characterized by dynamic light scattering (DLS) using a Zetasizer Nano ZS from Malvern Instruments. The micelle sizes in the microemulsion as well as the hydroxide particle size after ammonia addition were measured at 25 °C. For DLS experiments, the measured viscosities of microemulsions were used. The average particle diameters ($z$-average) were determined from intensity weighted size distributions, calculated using the non-negative least squares algorithm.

Samples for transmission electron microscopy (TEM) analysis were prepared by dipping carbon coated copper grids into microemulsions containing $Ce(OH)_3$ particles. TEM investigations were performed on the Cs-corrected 200 kV-TEM FEI Tecnai F20 Cs-corr at the Triebenberg Laboratory for high resolution TEM and electron holography. Cs-correction was used for a precise estimation of the lateral dimensions to avoid errors induced by delocalization effects caused by a high spherical aberration. Field emission scanning electron microscopy (FESEM) on a fractured surface of pyrolyzed composites was carried out with a Stereoscan 260 SEM with an energy dispersive X-ray (EDX) spectra analysis system using a backscattered electron (BSE) detector. X-ray powder diffraction patterns were recorded in transmission geometry using a Stoe Stadi-P diffractometer and Cu K$\alpha_1$ radiation ($\lambda = 0.15405$ nm). Netzsch STA-409 and STA-429 instruments were used for thermal analyses. The precursor systems were heated in a corundum crucible up to 1550 °C with 10 °C/min in argon and in air atmosphere.

Nitrogen physisorption isotherms were measured at −196 °C using a Quantachrome Novasorb 2000 apparatus. Prior to the measurement, the samples were activated in vacuum at 200 °C for 5 h. Specific surface areas were calculated using the Brunauer−Emmett−Teller equation ($p/p_0 = 0.05$–$0.2$). The pore size distribution was estimated from the desorption branch of the isotherm using the Barrett−Joyner−Halenda (BJH) theory.

## Results and Discussion

**Microemulsions.** The formation of the cerium hydroxide particles in micelles (Scheme 1, step A) was followed using DLS. By changing the $R_W$ value ($R_W$ is the molar ratio of water to surfactant, see also Table S1 in the Supporting Information), we were able to control the hydrodynamic diameter of particles from 2.0 to 9.9 nm. The resulting particles had low polydispersity indices (PDIs) between 0.08 (for $R_W = 5.8$) and 0.12 (for $R_W = 16.4$), indicating a relatively narrow particle size distribution. As expected, the particle size was increasing with increasing $R_W$ (Figure 1). For $R_W$ values higher than 16.4, the microemulsions became unstable after addition of ammonia (Scheme 1, step A) and lost transparency. Thus, for the preparation of the $CeO_X$/SiC nanocomposites (Scheme 1, step B), microemulsions with $R_W$ values of 5.8, 11.7, and 16.4 were used (Table 3). Time dependent DLS measurements (Figure 2) showed that the particle size increases with time for systems with high $R_W$ values. For example, the average particle diameter increases from 9.8 to 11.4 nm within 10 h after addition of ammonia for $R_W = 16.4$. On the other hand, microemulsions

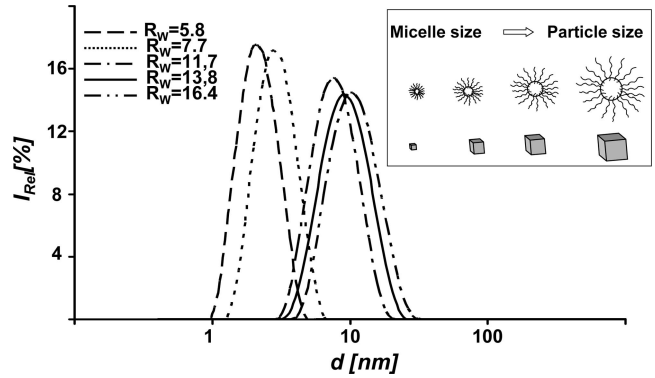


**Figure 1.** DLS measurements of the microemulsion systems with different $R_W$ values after ammonia addition.

**Table 3. Preparation Parameters and Specific Surface Areas before and after Oxidation of the $SiC/CeO_2$ Nanocomposites Pyrolyzed at Different Temperatures with Theoretical $SiC/CeO_2$ Ratio of 36 for Different $R_W$ Values in Microemulsions**

| | | | specific surface area [m$^2$ g$^{-1}$] | |
|---|---|---|---|---|
| sample name | $R_W$ | $T^a$ [°C] | after pyrolysis | after oxidation |
| A5.8-1200 | 5.8 | 1200 | 2 | 2 |
| A5.8-1350 | 5.8 | 1350 | 2 | 85 |
| A5.8-1500 | 5.8 | 1500 | 27 | 97 |
| A11.7-1200 | 11.7 | 1200 | 48 | 27 |
| A11.7-1350 | 11.7 | 1350 | 102 | 86 |
| A11.7-1500 | 11.7 | 1500 | 74 | 12 |
| A16.4-1200 | 16.4 | 1200 | 106 | 62 |
| A16.4-1350 | 16.4 | 1350 | 240 | 132 |
| A16.4-1500 | 16.4 | 1500 | 46 | 43 |

[a] Pyrolysis temperature (ramp 5).

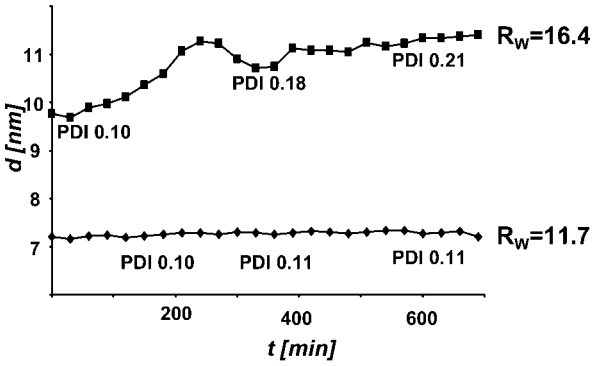


**Figure 2.** Time resolved particle sizes for the microemulsion systems with $R_W$ values of 11.7 and 16.7, after ammonia addition (step A).

with a low $R_W$ value of 11.7 were more stable, and the particle size remained constant over the same time period. Also, the PDI for the sample with high $R_W$ value (16.4) increased significantly within this time from 0.10 to 0.21, indicating severe agglomeration. For the sample with low $R_W = 11.7$, the ripening process was milder and the PDI increased only slightly from 0.10 to 0.11.

After ammonia addition (Scheme 1, step A), the microemulsion system with $R_W = 16.4$ was characterized using TEM. Figure 3 shows regular particles in the range of 2–3 nm with spherical shapes. Lattice fringes can be observed in high-resolution TEM images (Figure 3C). The *d*-spacing in Figure 3C was determined as 3.23, 2.78, and 1.99 Å corresponding to the (110), (200), and (002) *d*-spacing of cerium hydroxide (3.250 Å, 2.820 Å, and 1.914 Å[37]).

**Microemulsions with Polycarbosilane.** After addition of polycarbosilane, the nanoparticle solution remained clear (Scheme 1, step B). The polycarbosilane was preferentially dissolved in the oil phase (heptane). The latter was subsequently removed via evaporation in a vacuum (together with water) (Scheme 1, step C). Depending on the evaporation conditions, the product was either liquid or solid (Scheme 1, step C]. High evaporation temperatures (150 °C) resulted in solid products, whereas a liquid was obtained for lower temperatures (80 °C). The latter indicates that hydrosilylation reactions initiated at higher temperatures caused cross-linking and solidification of the liquid polycarbosilane precursor containing functional allyl groups.[38] The incomplete removal of heptane is not the reason for the differences in viscosity because the weight loss for both evacuation temperatures was the same. The same effect was also observed at room temperature for the catalytic hydrosilylation with $H_2PtCl_6$.[39] For our further studies reported here, only solid samples evacuated at 150 °C were used without addition of the platinum catalysts.

The remaining polycarbosilane/surfactant/cerium hydroxide composites were pyrolyzed in an argon flow at different temperatures (from 1200 to 1500 °C; see also Figure S2 in the Supporting Information; Scheme 1, step D) and subsequently oxidized at 900 °C to remove the residual carbon impurities (Scheme 1, step E). The temperature range for the pyrolysis and oxidation was chosen on the basis of thermogravimetric (TG) measurements and will be discussed further in detail.

Table 3 summarizes the measured specific surface areas after pyrolysis and oxidation for the preparation of $CeO_X$/SiC nanocomposites (with constant $SiC/CeO_2$ theoretical mass ratio of 37). The highest specific surface areas were typically observed for the samples pyrolyzed at a moderate temperature of 1350 °C, with a maximum value of 240 $m^2\ g^{-1}$ measured for A16.4-1350. Samples prepared with the lowest $R_W$ value of 5.8 showed the highest specific surface areas when pyrolyzed at 1500 °C (27 $m^2\ g^{-1}$ for the A5.8-1500 sample). However, the specific surface area increases significantly after the oxidation at 900 °C (e.g., from 27 to 97 $m^2\ g^{-1}$ for the A5.8-1500 °C sample). This is in contrast to the samples with the $R_W$ of 11.7 and 16.4 which show a decrease in the specific surface area because of the oxidation (e.g., from 74 to 12 $m^2\ g^{-1}$ for A11.7-1500 or from 46 to 43 $m^2\ g^{-1}$ for A16.4-1500). The latter is a consequence of the high amount of surfactant used in the microemulsion with the lowest $R_W$ value (to keep the constant $CeO_X$ loading, the $R_W$ value was controlled by changing the surfactant content). The large amounts of carbonized surfactant probably functioned as an endotemplate resulting in the formation of porosity upon oxidative removal in air (eq 1).[40]

$$C + O_2 \rightarrow CO_2 \quad (1)$$

The decrease of specific surface area after oxidation for samples prepared with the high $R_W$ values (11.7 and 16.4) is caused by silicon carbide oxidation resulting in a thin $SiO_2$ surface layer. Typically, higher specific surface areas cause higher oxidation rates.[36]

$$SiC + 2O_2 \rightarrow SiO_2 + CO_2 \quad (2)$$

Samples with the highest specific surface area (A16.4-1350) show type IV nitrogen adsorption isotherms with a hysteresis loop (Figure 4). The average pore diameter of 3.5 nm before and 4.5 nm after oxidation was calculated via the BJH theory from the desorption branch.

For comparison, also samples with a higher $CeO_X$ loading ($SiC/CeO_2$ mass ratio of 18.5) as well as one derived from the pure polycarbosilane precursor were investigated. Table 4 summarizes the pyrolysis conditions and the measured specific surface areas of the cerium rich samples and those prepared from the pure polycarbosilane. Cerium rich samples pyrolyzed at low temperatures (1200 and 1350 °C) have lower specific surface areas (Table 4) than the composites with a low metal content (Table 3). The sample pyrolyzed at 1500 °C has a surface area (43 $m^2\ g^{-1}$, B16.4-1500) similar to that of the low cerium content material (46 $m^2\ g^{-1}$).

After oxidation, the surface area of samples with high cerium loading prepared at 1200 and 1500 °C decreases while the specific surface area increases for the sample pyrolyzed at 1350 °C (Table 4). Reference SiC materials prepared directly from the pure polycarbosilane precursor had sig-

(37) Christensen, A. N. *Acta Chem. Scand.* **1966**, *20*, 896.
(38) Marciniec, B.; Gulinski, J.; Urbaniak, W.; Kornetka, Z. W. *Comprehensive Handbook on Hydrosilylation*; Pergamon Press: Oxford, 1992.
(39) Speier, J. L.; Webster, J. A.; Barnes, G. H. *J. Am. Chem. Soc.* **1957**, *79*, 974.
(40) Schüth, F. *Angew. Chem., Int. Ed.* **2003**, *42*, 3604.

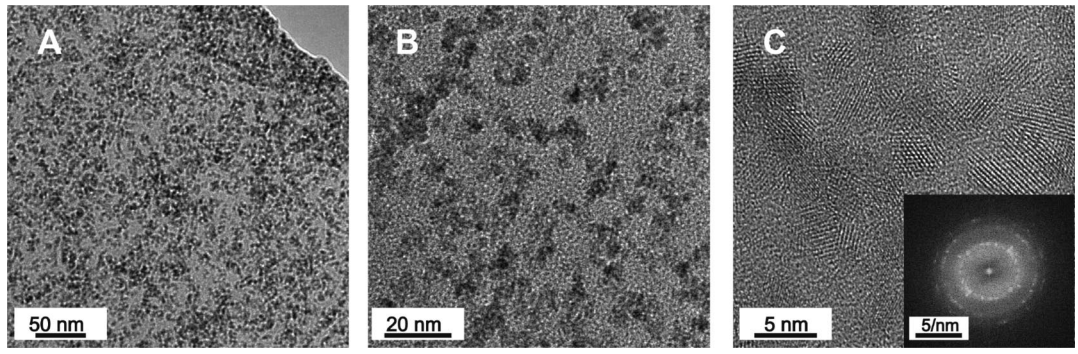


**Figure 3.** TEM images of the $Ce(OH)_3$ nanoparticles with $R_W$ of 16.4 after ammonia addition.

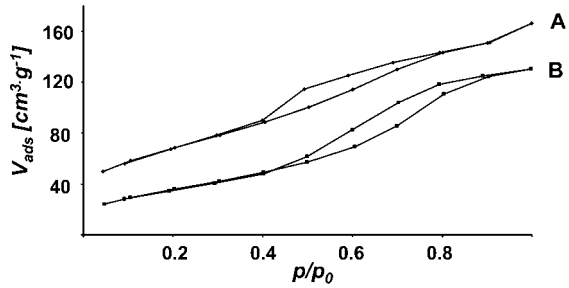


**Figure 4.** Nitrogen physisorption measurements for A16.4-1350 before (A) and after oxidative treatment at 900 °C (B).

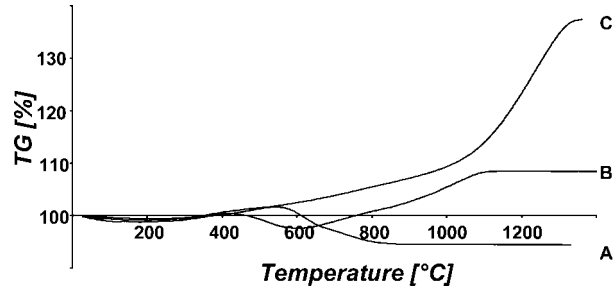


**Figure 5.** TG measurements of composite A16.4 pyrolyzed at (A) 1200 °C, (B) 1350 °C, and (C) 1500 °C.

**Table 4. Preparation Parameters and Specific Surface Area before and after Oxidation of the $SiC/CeO_2$ Nanocomposites with Theoretical $SiC/CeO_2$ Ratio of 18.5 For $R_W = 16.4$ and the SiC Ceramics of the Pure SMP-10 Precursor Pyrolyzed at Different Temperatures**

| | | | specific surface area [$m^2\ g^{-1}$] | |
|---|---|---|---|---|
| sample name | $R_W$ | $T^a$ [°C] | after pyrolysis | after oxidation |
| B16.4-1200 | 16.4 | 1200 | 6 | 3 |
| B16.4-1350 | 16.4 | 1350 | 61 | 91 |
| B16.4-1500 | 16.4 | 1500 | 43 | 33 |
| SMP-10-1200 | | 1200 | <1 | <1 |
| SMP-10-1350 | | 1350 | <1 | <1 |
| SMP-10-1500 | | 1500 | 4 | <1 |

[a] Pyrolysis temperature (ramp 5).

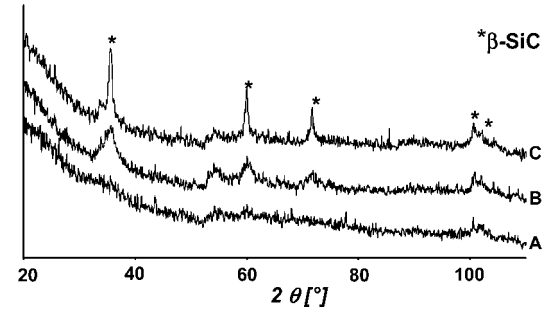


**Figure 6.** X-ray diffraction patterns of the $SiC/CeO_x$ samples pyrolized at various temperatures: (A) 1200, (B) 1350, and (C) 1500 (before oxidation) A16.4.

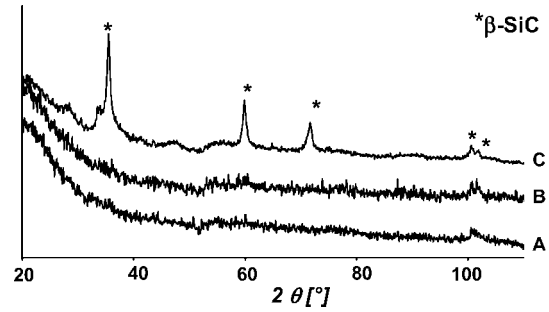


**Figure 7.** X-ray diffraction patterns of the $SiC/CeO_x$ samples A16.4 after oxidation at 900 °C pyrolized at various temperatures: (A) 1200, (B) 1350, and (C) 1500.

nificantly lower specific surface area (1–4 $m^2\ g^{-1}$) than all composite materials prepared via the microemulsion procedure. The specific surface areas of $CeO_X$/SiC composites are moderate or relatively low as compared to those of the high surface area silica materials with surface areas up to 1000 $m^2\ g^{-1}$. However, only a few materials maintain such high surface areas at temperatures up to 1500 °C. In this context, the surface areas are relatively high as compared to those of other materials such as $BaAl_{12}O_{19}$. Additionally, for long term stability and oxidation resistance, surface areas in a range of 50–100 $m^2\ g^{-1}$ are beneficial.

TG measurements showed a different oxidation behavior of $SiC/CeO_X$ samples pyrolyzed at various temperatures (A16.4: Figure 5, B16.4; see also Figure S3 in the Supporting Information). The final mass gain at 1300 °C was increasing with increasing pyrolysis temperature. For the sample prepared at 1500 °C (A16.4-1500), a mass gain of 38 wt % was observed while a weight loss of 7 wt % (A16.4-1200) was measured for the sample pyrolyzed at 1200 °C. The high mass gain of A16.4-1500 can be due to the SiC oxidation (eq 2) because the high surface area SiC is known to oxidize at lower temperatures as compared to that of the bulk SiC.[32,36] On the other hand, A16.4-1200 in the first step loses weight (~7 wt %) because of the carbon oxidation at around 600 °C, and then the mass remains constant. The latter can be caused by the overlapping temperature regimes for free carbon and SiC oxidation.

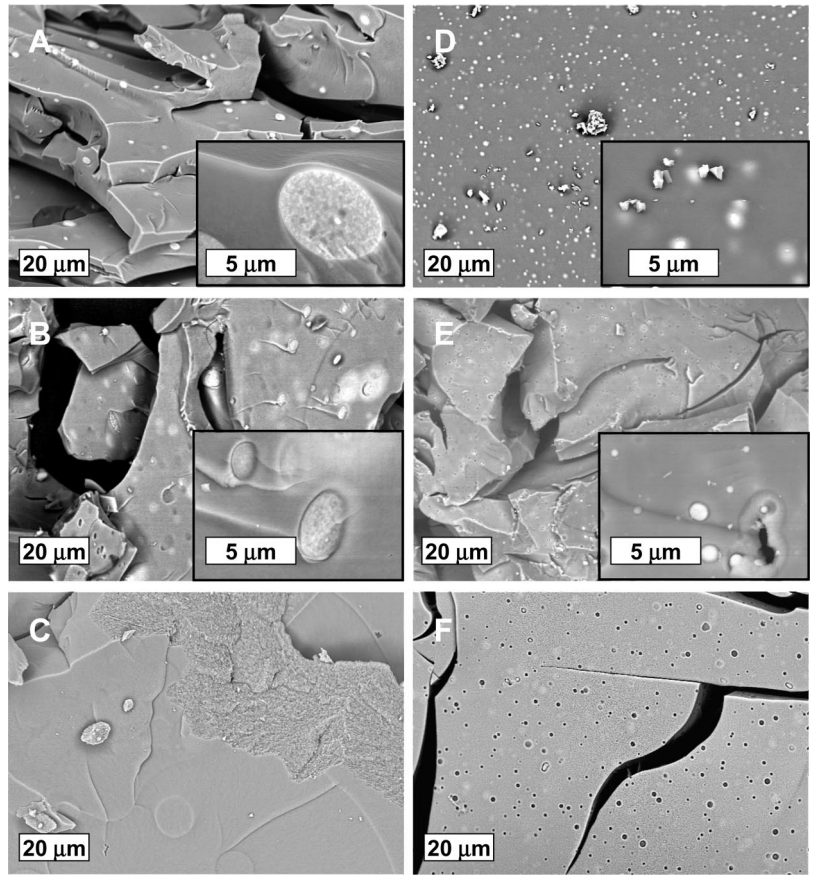


**Figure 8.** FESEM of the composites A16.4 pyrolyzed at 1200 °C (A), 1350 °C (B), and 1500 °C (C) and B16.4 at 1200 °C (D), 1350 °C (E), and 1500 °C (F).

**Table 5. Elemental Composition of Pyrolyzed $CeO_X$/SiC Composites (by EDX)**

| | wt % (A16.4-1200) | | wt % (B16.4-1200) | |
|---|---|---|---|---|
| element | calculated | observed[a] | calculated | observed[a] |
| silicon | 68.2 | 30.2 | 66.1 | 23.8 |
| carbon | 29.1 | 53.3 | 28.3 | 57.3 |
| cerium | 2.2 | 1.5 | 4.5 | 1.9 |
| oxygen | 0.5 | 25.0 | 1.1 | 17.0 |

[a] Mean values of four EDX measurements (at magnification of 1000).

The X-ray diffraction patterns of A16.4 show the increasing crystallinity of mainly cubic $\beta$-SiC (JCPDS: 73-1665) with increasing pyrolysis temperature (Figure 6). Some small amounts of other SiC polytypes were detected, but no reflections of $CeO_2$ could be measured for any of the samples (probably because of the low loading of the metal). The oxidative treatment of samples at 900 °C resulted in the oxidation of SiC prepared at 1200 (A16.4-1200 O) and 1350 °C (A16.4-1350 O), and no peaks of crystalline SiC were observed (Figure 7). However, for the sample A16.4-1500 prepared at 1500 °C, the $\beta$-SiC phase could be still detected after postoxidative temperature annealing. Thus, the high surface area SiC with poor crystallinity is not stable enough to sustain a high temperature oxidative treatment, whereas the moderate surface area material A16.4-1500 is more suitable as a catalyst support in oxidation catalysis.

FESEM images of low (A16.4) and high ceria content sample (B16.4) with $R_W = 16.4$ prepared at various temperatures are presented in Figure 8. Low pyrolysis temperatures result in SiC materials with macroporous structure with visible aggregates of $CeO_X$ particles (Figure 8A,D ). If the pyrolysis temperature is increased to 1500 °C (Figure 8C), the $CeO_X$ particles disappear and most probably form an amorphous cerium silicate. This is even more visible for samples with a higher $CeO_X$ loading where one can observe the formation of the small pores in the SiC structure resulting from the $CeO_X$ particles (Figure 8F).

Materials prepared with lower $R_W$ values and low $CeO_X$ concentration show a lower amount of particles present on the surface of SiC (for samples prepared at 1200 °C). They also showed the formation of pores in regions where $CeO_X$ particles were observed (FESEM A5.8, 11.7: see also Figure S4 in the Supporting Information).

Semiquantitative elemental analyses were obtained using EDX spectroscopy (Table 5). The elemental composition of the pyrolyzed $CeO_X$/SiC composite differs from the theoretical ratio. The oxygen and carbon contents are significantly higher than expected. The reason for these higher fractions can be explained by the residual carbon resulting from the surfactant carbonization. These results are in agreement with the mass losses caused by the removal of residual surfactant in the $CeO_X$/SiC ceramics by the postoxidative treatments in air (Figure 5, eq 1). High content $CeO_X$ composites with a higher surfactant ratio (B16.4-1200) have significantly higher carbon fractions of 57.3 wt % as compared to composites with a lower cerium oxide content (A16.4-1200, 53.3 wt % carbon). However, also the oxygen content of

B16.4-1200 with 25.0 wt % indicates a higher silica content than in A16.4-1200 with a 17.0 wt %. The higher carbon and oxygen content is also a reason for the lower silicon content (A16.4-1200: 30.2 wt % measured, 68.2 wt % calculated) and cerium content (A16.4-1200: 1.5 wt % measured, 2.2 wt % calculated). Whereas the relative cerium content reasonably reflects the starting composition, the interpretation of the light element analyses by EDX should not be overstated, given the limitations of the EDX method.

## Conclusions

Summarizing, we have presented a new method for the incorporation of $CeO_X$ nanoparticles during the synthesis of SiC from the polymer precursors using microemulsion techniques and a polycarbosilane as the SiC precursor. By varying the $R_W$ value, the particle size can be controlled in the microemulsion system. Different pyrolysis temperatures were used to synthesize porous SiC composite structures with different metal oxide loadings and surface areas up to 240 $m^2\ g^{-1}$. The state of the precursor system from solid to liquid ($CeO_X$/polycarbosilane/surfactant) can be controlled by changing the processing temperature and by addition of a catalyst. This can be especially useful for the preparation of bulk or film structures. $CeO_X$/SiC materials prepared via microemulsion techniques can also be potential catalysts in oxidation reactions. The catalytic properties are currently being studied and will be reported in a separate contribution.

**Acknowledgment.** Financial support by the German Research Foundation (KA 1698/6-1 and HE 2457/12-1) in the NanoMat Program SPP 1181 is gratefully acknowledged.

**Supporting Information Available:** An additional table and four figures that contain the following material: (S1) average hydrodynamic diameter and PDI, (S2) thermogravimetric measurements for pyrolysis, (S3) thermogravimetric measurements of the composite B16.4, (S4) FESEM of the composite A11.7, and (S5) EDX of composite structures (PDF). This material is available free of charge via the Internet at http://pubs.acs.org.

CM071657N